Pergamon

Int. J. Solids Structures Vol. 32, No. 23, pp. 3423–3434, 1995

0020–7683/95 $9.50 + .00

0020–7683(94)00315–7

PREDICTION OF DEFORMATION BEHAVIOR OF GLASSY POLYMERS BASED ON MOLECULAR CHAIN NETWORK MODEL

Y. TOMITA and S. TANAKA
Faculty of Engineering, Kobe University, Kobe, Japan

(*Received* 20 *July* 1994)

Abstract—In order to develop a constitutive equation for polymeric materials covering a wide class of deformation processes a three-dimensional nonaffine model has been developed by adopting the non-Gaussian network theory with the generalized Argon double-kink model of intermolecular resistance. A phenomenological relation between the non-Gaussian molecular chain network structure and entanglement of chains is formulated and a simple evolutional equation of the number of entanglements of chains during the deformation process is developed. The validity of the proposed constitutive equation has been proven through comparison between the predicted results and experimental results. Furthermore, its application to the deformation analysis of circular polymeric bars under tension has been discussed

1. INTRODUCTION

Deformation behavior of polymeric material under tension is unique. Necking initially develops in the specimen and subsequently propagates along the specimen under an essentially steady-state condition, of which characteristic feature is technically utilized to produce tapes, films and fibers. This typical deformation behavior can be phenomenologically explained by the marked restiffening of the stress–strain relation at a specific point (Hutchinson and Neale, 1983). The mechanical aspect of this phenomenon has recently received much attention. Hutchinson and Neale (1983) and Chater and Hutchinson (1984) investigated neck propagation in tension blocks, bulge propagation in long cylindrical balloons and buckle propagation of tubes under lateral pressure in terms of simple one-dimensional analysis. In further studies, full finite element analyses for a solid circular bar (Neale and Tugcu, 1985), plane strain blocks (Fager and Bassani, 1986; Tugcu and Neale, 1987a), and neck and bulge propagation with respect to circumferential and axial direction (Tomita *et al.*, 1990) have been conducted. In subsequent studies, the effect of strain rate (Tugcu and Neale, 1987a,b, 1988) and temperature (Tugcu and Neale, 1990) sensitivities on neck propagation have been clarified. Tomita and Hayashi (1991, 1993) clarified thermocoupled elasto-viscoplastic neck propagation behavior.

On the other hand, from the physical point of view, the hardening characteristics in the glassy polymer are generally explained by the alignment of molecular chains, which are randomly oriented in the undeformed state and are responsible for neck development and its propagation, and deformation-induced anisotropy. Rather intensive research has been carried out on this subject. Several three-dimensional models have been developed by adopting the non-Gaussian affine network model with the generalized Argon double-kink model (Argon, 1973). Among them are the three-chain (Boyce *et al.* 1988; which we shall term the BPA model). Eight-chain (Arruda and Boyce, 1991, 1993a) and full network models (Wu and van der Giessen, 1993a). The validity of these models was examined in terms of the predictability of the experimentally observed deformation behaviors (Arruda and Boyce, 1991, 1993a; Wu and van der Giessen, 1993a), and it was clarified that the deformation behavior of polymeric material under tension and compression are well predicted, whereas substantial differences are observed in simple shear deformation. This is partially attributed to the difference in the development of internal microstructures, depending on the stress system induced.

In the preliminary investigations (Tanaka and Tomita, 1993, 1994), we attempted to establish a nonaffine network model where the number of entanglements, i.e. connecting points of molecular chains, changes depending on the local stress system, and discussed the capability of the prediction of deformation behavior of polymeric material under different stress systems. Here, in order to develop a constitutive equation covering a wide class of deformation processes, a relation between the non-Gaussian molecular chain network structure and entanglements of chains is formulated and a simple evolutional equation of the number of entanglements of chains during the deformation process is developed. The validity of proposed constitutive equation and its application to the deformation analysis of tension in cylindrical polymeric bars will be discussed.

2. CONSTITUTIVE EQUATION

2.1. *Affine model*

Plastic flow of glassy polymer is assumed to start when stress exceeds the resistances to rotation of segments of the molecular chain and its alignment. Argon (1973) developed the constitutive equation for the plastic shear strain rate, $\dot{\gamma}^{\mathrm{p}}$, which occurs once the isotropic barrier to chain segment rotation has been overcome:

$$\dot{\gamma}^{\mathrm{p}} = \dot{\gamma}_{\mathrm{o}} \exp[(-As_{\mathrm{o}}/T)\{1-(\tau/s_{\mathrm{o}})^{5/6}\}], \tag{1}$$

where $\dot{\gamma}_{\mathrm{o}}$ and A are constants, T is absolute temperature, $s_{\mathrm{o}} = 0.077G/(1-\upsilon)$ is the athermal shear strength, G is the elastic shear modulus, υ is Poisson's ratio and τ is the applied shear stress. Boyce *et al.* (1988) extended this expression to include the effect of pressure. They used $s+\alpha p$ instead of s_{o}, where s is the shear stress which evolves with the plastic strain from s_{o} to a stable value, s_{ss}, p is the pressure and α is a pressure-dependent coefficient. Since s depends on temperature and strain rate, the evolutional equation of s can be expressed by

$$s = h\{1-(s/s_{\mathrm{ss}})\}\dot{\gamma}^{p}, \tag{2}$$

where h is rate of resistance with respect to plastic strain, and s_{ss} is the stable saturation value of s_{o}. Here, in order to duplicate the response of various polymeric materials after yielding, shown in Fig. 1, the value of s_{ss} is adjusted according to the materials (Tomita, 1994).

Once the polymeric materials experience a stress that exceeds their intermolecular resistance, the molecular chains align along the principal direction of plastic stretch. This alignment generates the back-stress. The initial structure of the molecular chain networks is assumed to be isotropic. After yielding, the molecular chains will be stretched and will tend to align along the principal direction of plastic stretch. The principal component of

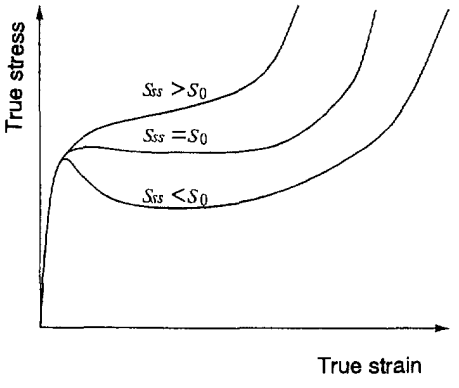

Fig 1. True stress–natural strain relations with/without work hardening and softening polymeric materials

back-stress is taken to the coaxial with the plastic stretch tensor. The principal components of the back-stress tensor for the eight-chain model (Arruda and Boyce, 1991, 1993a) are

$$\begin{aligned} B_i &= C^R \lambda_L L^{-1}(V^p/\lambda_L)(V_i^{p2} - V^{p2})/V^p/3 \\ L^{-1}(V^p/\lambda_L) &= x \\ L(x) &= \coth x - x^{-1} = V^p/\lambda_L \\ V^{p2} &= (V_1^{p2} + V_2^{p2} + V_3^{p2})/3, \end{aligned} \tag{3}$$

where B_i is the principal component of back-stress, V_i^p is principal plastic stretch, $\lambda_L = \sqrt{N}$ is the locking stretch in tension, N is average number of kinks in a single chain, $C^R = nkT$ is a constant, n is the number of chains in the unit volume, k is Boltzmann's constant, and L is the Langevin function. In the affine model, the entangled points of molecular chains are assumed to be the connecting points and their number, in other words, the number of chains in the unit volume n and the average number of kinks in a single chain N, are assumed to be unchanged during the deformation. The back-stresses for the three-chain model (Boyce *et al.*, 1988) and full network model (Wu and van der Giessen, 1993a) have been derived.

The deformation gradient $\mathbf{F}$ from the initially isotropic state of polymer can be decomposed into the elastic part $\mathbf{F}^e$ and plastic part $\mathbf{F}^p$. $\mathbf{F}^p$ represents the relaxed configuration obtained by unloading without rotation and permanent orientation of molecular alignment. In the BPA model (Boyce *et al.*, 1988), the magnitude of the plastic deformation rate tensor $\mathbf{d}^p$ is assumed to be given by representative plastic shear strain rate $\dot{\gamma}^p$, and the direction is specified by the normalized deviatoric part of driving stress σ^*. Then

$$\begin{aligned} \mathbf{d}^p &= \dot{\gamma}^p \boldsymbol{\sigma}^{*\prime}/\sqrt{2}\tau \\ \sigma^* &= \sigma - \mathbf{F}^e\mathbf{B}\mathbf{F}^{e-1}/\det\mathbf{F}^e \\ \tau &= (\sigma^*\sigma^*/2)^{1/2}, \end{aligned} \tag{4}$$

where σ is the Cauchy stress tensor, $\mathbf{B}$ is the back-stress tensor with principal values B_i in eqn (3). The shear stress τ in eqn (1) is estimated by τ in eqn (4). The complete elastic–plastic constitutive equation can be established by introducing the elastic constitutive equation for the elastic part of the deformation rate tensor:

$$\overset{\nabla}{\mathbf{S}} = \mathbf{D}^e(\mathbf{d} - \mathbf{d}^p) = \mathbf{D}^e\mathbf{d} - \mathbf{D}^e\dot{\gamma}^p\sigma^{*\prime}/2\tau, \tag{5}$$

where $\overset{\nabla}{\mathbf{S}}$ is the Jaumann rate of Kirchhoff stress, $\mathbf{D}^e$ is elastic stiffness and $\mathbf{d}$ is the deformation rate tensor. In all computations presented in this investigation, the elastic strain remains small and all geometrical changes associated with the elastic part of the deformation are neglected (see Boyce *et al.*, 1988; Wu and van der Giessen, 1993a).

2.2. *Nonaffine model*

In the BPA and other models, entangled points of polymeric chains are assumed to be connecting points which are unchanged during the deformation processes. In real deformation processes, however, the number of entangled points may increase or decrease according to the local deformation of the polymeric chain (Botto *et al.*, 1987). Increase of the entangled points reduces the number of kinks in polymeric chains, which causes the reduction of extensibility and increase in the relative stiffening of the materials. On the

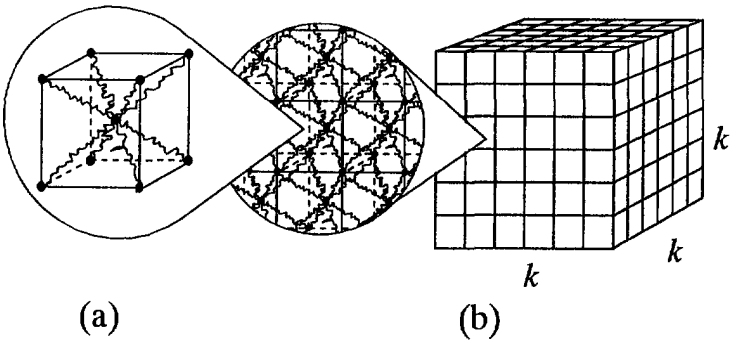

Fig 2. Eight-chain model (a) and material element constituting of k^3 pieces of eight-chain models (b).

other hand, decrease of entangled points causes the opposite effects. According to the eight-chain model shown in Fig. 2(a), the relation between the number of molecular chains and entangled points will be formulated. Here, a material element consisting of molecular chains is assumed as a block constituted of k^3 pieces of eight-chain models, as shown in Fig. 2(b). The corresponding number of chains and entangled points (connecting points) in the block are $n = 8k^3$ and $m = (k+1)^3 + k^3$, respectively. For a sufficiently large number of k, we have

$$m = n/4. \tag{6}$$

Next, we assume that the total number of kinks in the blocks is preserved during the deformation. With total number of kinks in the block N_A and average total number of kinks in a single chain N, the following relation is obtained

$$N_A = nN. \tag{7}$$

This provides the kink number in a single chain as

$$N = N_A/n = N_A/4m. \tag{8}$$

The limiting stretch for a chain is $\sqrt{N}$ and $N > 1$, which specifies the limiting number of entangled points m_{ult}:

$$m_{ult} = N_A/4 > m. \tag{9}$$

The entanglement situation may change according to the local deformation behavior of polymeric material.

Here, in order to formulate the evolutional equation of the number of entanglements, we introduce the molecular chain field shown in Fig. 3. The molecular chain network aligns

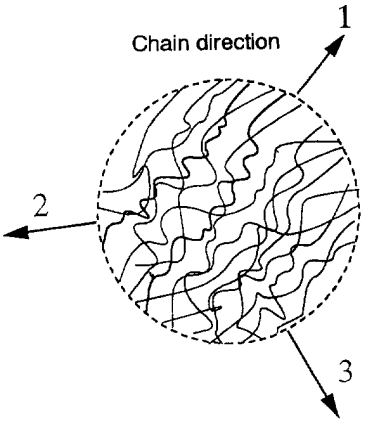

Fig 3. Hypothetical model of chain-field and orthogonal coordinate system.

in the principal direction of plastic stretch (Wu and van der Giessen, 1993a), which is unchanged for uniaxial tension and compression. The first direction of the orthogonal coordinates shown in Fig. 3 is set to be the direction of maximum principal plastic stretch. Hereafter, this direction will be called the chain direction. Then we define the orthogonal coordinate system parallel to the principal direction of plastic stretch tensor shown in Fig. 3. The tensile deformation applied to the chain direction causes the extension of the chain and increase of the stiffness. It simultaneously reduces the relative distance of adjacent chains, which may induce the entanglements. The similar situation can be adopted for the case of compressive deformation perpendicular to the chain direction. On the other hand, the tensile deformation perpendicular to the chain direction increases the relative distance of adjacent chains, which may reduce the entanglements. A similar situation can be expected for compression parallel to the chain direction. For the shear deformation with respect to the orthogonal coordinate direction, the direction of the principal plastic stretch rotates, which causes rotation of the molecular chain network (Wu and van der Giessen, 1993a) with respect to the remainder. This may cause the disentanglement. The above characteristic feature of the deformation of the molecular chain network can be summarized as follows

(1) The extension along the chain direction and the compression perpendicular to the chain direction increase the number of entanglements and vice versa.

(2) The shear deformation parallel to the orthogonal coordinate system reduces the number of entanglements.

An evolutional equation of the number of entanglements is determined by the local deformation of the polymer and may be expressed as

$$\dot{m} = \chi_{ij}(T)\dot{\varepsilon}_{ij}^{\mathrm{p-ch}}, \tag{10}$$

where $\chi_{ij}(T)$ is the tensor depending on the temperature, and $\dot{\varepsilon}_{ij}^{\mathrm{p-ch}}$ is the plastic strain rate tensor with respect to the chain coordinate system. From the above discussion, we may obtain the following simple concrete form of eqn (10).

$$\dot{m} = \chi_{11}\dot{\varepsilon}_{11}^{\mathrm{p-ch}} - \chi_{22}\dot{\varepsilon}_{22}^{\mathrm{p-ch}} - \chi_{33}\dot{\varepsilon}_{33}^{\mathrm{p-ch}} - 2\chi_{12}|\dot{\varepsilon}_{12}^{\mathrm{p-ch}}| - 2\chi_{23}|\dot{\varepsilon}_{23}^{\mathrm{p-ch}}| - 2\chi_{31}|\dot{\varepsilon}_{31}^{\mathrm{p-ch}}|, \quad \chi_{ij} > 0. \tag{11}$$

This equation implies that the extension along the chain direction and the compression perpendicular to the chain direction cause the increase of the number of entanglements and vice versa. The shear deformation, regardless of the direction, reduces the number of entanglements. Furthermore, assuming that the contributions of normal strain rate and shear strain rate on the increase or decrease of the number of entanglements are identical, and considering the limiting number of entanglements, we have

$$\begin{aligned} \chi_{11} &= \chi_{22} = \chi_{33} = c_1(T)(1 - m/m_{\mathrm{u}}) \\ \chi_{12} &= \chi_{23} = \chi_{31} = c_2(T)(1 - m/m_{\mathrm{l}}), \end{aligned} \tag{12}$$

where c_1 and c_2 are temperature-dependent positive constants, and m_{u} ($< m_{\mathrm{ult}}$) and m_{l} are upper and lower limits of the number of entanglements, respectively. Substitution of eqn (12) into eqn (11) yields

$$\dot{m} = c_1(1 - m/m_{\mathrm{u}})(\dot{\varepsilon}_{11}^{\mathrm{p-ch}} - \dot{\varepsilon}_{22}^{\mathrm{p-ch}} - \dot{\varepsilon}_{33}^{\mathrm{p-ch}}) + 2c_2(1 - m/m_{\mathrm{l}})(|\dot{\varepsilon}_{12}^{\mathrm{p-ch}}| + |\dot{\varepsilon}_{23}^{\mathrm{p-ch}}| + |\dot{\varepsilon}_{31}^{\mathrm{p-ch}}|). \tag{13}$$

With n and N estimated using eqn (6)–(9) and eqn (13), the concrete constitutive equations for the three-dimensional deformation behavior can be established along the same lines as eqn (5).

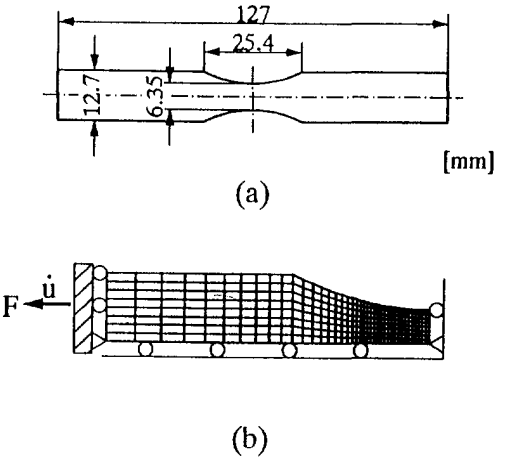

Fig 4. Computational model of cylindrical specimen under tension (a) and finite element discretization with crossed-triangular elements (b).

3. COMPARISON BETWEEN EXPERIMENTAL RESULTS AND COMPUTATIONAL PREDICTIONS

3.1. *Material parameters*

The material parameters for the eight-chain model used by Wu and van der Giessen (1993a) which were originally defined by Boyce and Arruda (1990) will be employed for the BPA model. They are $E = 2300$ MPa, $\nu = 0.30$, $s_o = 97.3$ MPa, $A = 240$ K MPa^{-1}, $\dot{\gamma}_o = 2.00 \times 10^{15}$ s^{-1}, $h = 500$ MPa, $s_{ss} = 73.9$ MPa, $\alpha = 0.08$, $C^R = 12.8$ MPa and $N = 2.15$. These values and eqns (6)–(8) with $T = 296$ K yield $N_A = 6.73 \times 10^{27}$ and $m_o = 7.83 \times 10^{26}$. Due to the lack of experimental results, it is very difficult to identify the values of m_1, c_1 and c_2. Provided $m_u = m_o$, m in eqn (13) vanishes and m remains constant for the deformation without shear, and the corresponding response for uniaxial deformation due to the BPA model is recovered so that the proposed model with $m_u = m_o$ is understood to be the extended version of the BPA model. According to finding (Wu and van der Giessen, 1993b) that the shear stress at very high strain has an almost identical value despite the different initial stage of deformation, we determined the constants m_1, c_1 and c_2 by trial and error such that the uniform simple shear deformation obtained by integrating constitutive equation (5) for the nonaffine model coincides with that from experiments (G'Sell and Gopez, 1985) in the high strain range. The additional parameters introduced in this paper are $m_1 = 0.34\, m_o$ and $c_1 = c_2 = 0.43\, m_o$.

3.2. *Computational model*

Figure 4 shows the cylindrical bar model employed by Boyce and Arruda (1990) (a) and finite element discretization with cross triangular elements (b). The deformation analysis is performed under constant temperature of 296 K and constant end velocity of 2.54 mm min^{-1}. Figure 5 shows the computational model for simple shearing of the plane strain block with unit thickness. To reveal the propagation of the shear band observed in the

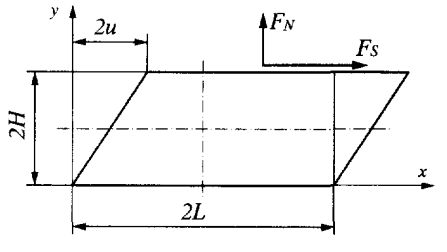

Fig 5. Computational model of block under shearing.

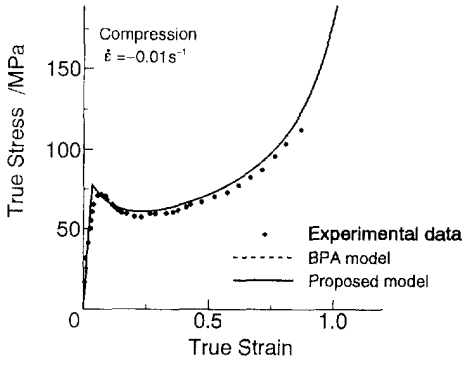

Fig 6. True stress versus strain relation under uniaxial compression. The experimental results are from Arruda and Boyce (1993b). The material parameters used for the simulation by using the BPA model are $E = 2300$ MPa, $\nu = 0.30$, $s_0 = 97.3$ MPa, $A = 240$ K MPa^{-1}, $\dot{\gamma}_0 = 2.00 \times 10^{15}$ s^{-1}, $h = 500$ MPa, $s_{ss} = 73.9$ MPa, $\alpha = 0.08$, $C^R = 12.8$ MPa and $N = 2.15$. In the proposed model, the material parameters employed are those for the BPA model plus $N_A = 6.73 \times 10^{27}$, $m_0 = 7.83 \times 10^{26}$, $m_u = m_0$, $m_1 = 0.34\, m_0$ and $c_1 = c_2 = 0.43\, m_0$.

experiments, the following initial imperfection Δs_0 in shear strength (Wu and van der Giessen, 1993b) has been introduced:

$$\Delta s_0 = -\zeta \exp\left[\{-(x-L)^2 + (L/H)^2(y-H)^2\}/\{0.01(L^2+H^2)\}\right], \tag{14}$$

where ζ is the initial imperfection. The finite element discretization employed is of a sufficiently fine uniform mesh with 60×12 quadrilaterals consisting of four crossed triangles. Normalized shear strain $\Gamma = u/H$, shear strain rate $\dot{\Gamma} = \dot{u}/H$ and shear stress $\sigma_s = F_s/L$ are introduced. The analysis has been performed at constant temperature of 296 K and shear strain rate $\dot{\Gamma} = 0.003$ s^{-1}. In order to avoid numerical instability near the softening region, the magnitude of the time step has been set such that $\Delta\gamma^p = \dot{\gamma}^p \Delta t < 0.0025$. With this imperfection, the shear band with high strain evolves at the center of the block and subsequently develops and extends normal to the shearing direction.

3.3. *Results and discussion*

Before considering the computational results under non uniform deformation, we will show the uniaxial true stress–strain relation for the material deformed at $T = 296$ K with nominal strain rate $\dot{\varepsilon} = 0.01$ s^{-1} in Fig. 6. The experimental results are from Arruda and Boyce (1993b). The numerical simulation using the BPA model has been performed applying the same material parameters discussed in section 3.1. As also discussed in section 3.1. the results obtained from the proposed model with $m_0 = m_u$ completely coincide with those from the BPA model, and good correspondence with the experimental results is observed.

Next, we will show the results of two-dimensional analysis of tension and shear deformation. The material parameters employed are the same as those employed in compression. Figure 7 shows the load normalized by maximum load (2349 N, obtained by

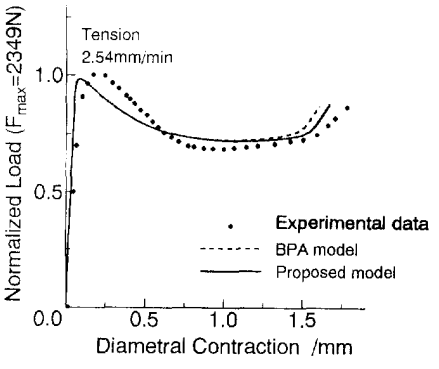

Fig 7. Normalized load versus diametral contraction. The notation and material parameters employed are the same as for Fig. 6. Experimental data are from Arruda and Boyce (1990).

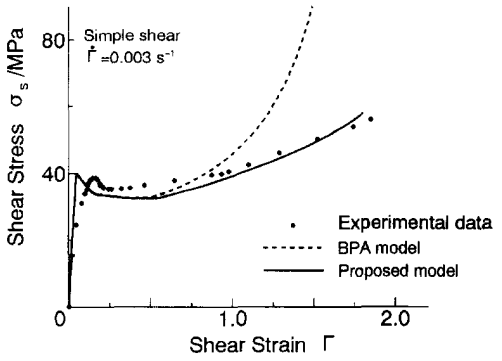

Fig 8. Shear stress versus shear strain. The experimental data are from G'Sell and Gopez (1985). The notation and material parameters employed are the same as for Fig. 6.

Boyce and Arruda, 1990) versus diametral contraction at the symmetric cross-section in the tension bar shown in Fig. 4(a). Although the maximum values of load predicted by the BPA model and proposed model are quite close, a discrepancy in the local deformation behavior over a rather small deformation range is observed. This is attributed to the simple assumption of an elastic response in the constitutive model, instead of real viscoplastic response. Good correspondence is observed in all cases over the neck propagation range with almost constant load. The difference observed in the results from BPA and proposed models in the later stage of deformation is due to the change in the number of entanglements.

Figure 8 shows the shear stress σ_s versus shear strain Γ relation. Again, due to the same reason as discussed above, a discrepancy between the theoretical prediction and experimental results (G'Sell and Gopez, 1985) is observed in the low deformation range. The computational predictions from the BPA model and proposed model are in good correspondence up to 0.5 in shear strain. However, overestimation of hardening is observed in the results from the BPA model. In the proposed model, the competitive effect of the hardening due to the extension of the polymeric chain and the softening caused by the disentanglement on the deformation behavior is suitably represented.

These results confirm the capability of the proposed model to predict the deformation behavior under different stress systems given a set of material parameters. In this respect, the proposed model is a natural generalization of the well-established models.

4. PARAMETRIC STUDY OF NECK PROPAGATION BEHAVIOR

With the proposed constitutive model, the effect of the introduced material parameter on the neck propagation behavior will be discussed.

4.1. *Computational model*

Figure 9 shows the computational model of cylindrical bars under uniform tension at both ends under a shear free condition. The nominal stress and strain are defined by

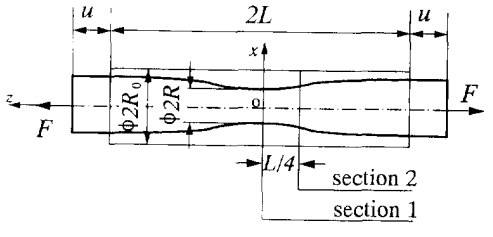

Fig 9. Computational model of tension of circular cylinder. The material parameters employed are $E/s_0 = 23.6$, $s_{ss}/s_0 = 1.20$, $h/s_0 = 15.4$, $As_0/T = 65.7$, $\nu = 0.30$, $\alpha = 0.0$, $\dot{\gamma}_0 = 2.00 \times 10^{15}\,s^{-1}$, $s_0 = 97.3$ MPa, $T = 296$ K, $N_A = 2.74 \times 10^{27}$, $m_a = 1.71 \times 10^{26}$, $c_0 = 7.38 \times 10^{26}$, $\zeta = 0.005$, $m_u = m_a$ and $m_l = m_a/3$ where m_a is the reference number of entangled points and c_0 is the reference value of c_1 and c_2 in eqn (13).

$\sigma_n = F/\pi R_o^2$ and $\varepsilon_n = u/L$, respectively. In order to ascertain the starting point of necking, the following initial geometrical imperfection is introduced:

$$R = R_o(1-\zeta), |z| < L/4, \tag{15}$$

where ζ is the initial imperfection. The material and computational parameters employed are $E/s_o = 23.6$, $s_{ss}/s_o = 1.20$, $h/s_o = 15.4$, $As_o/T = 65.7$, $\nu = 0.30$, $\alpha = 0.0$, $\dot{\gamma}_o = 2.00 \times 10^{15}$ s^{-1}, $s_o = 97.3$ MPa, $T = 296$ K, $N_A = 2.74 \times 10^{27}$, $m_a = 1.71 \times 10^{26}$, $c_o = 7.38 \times 10^{26}$, $\zeta = 0.005$, $m_u = m_a$ and $m_l = m_a/3$ where m_a is the reference number of entanglements and c_o is the reference value of c_1 and c_2 in eqn (14). The initial number of entanglements m_o and c_1/c_2 will be changed to clarify the effect of these values of the neck propagation behavior. The finite element discretization similar to that shown in Fig. 4 is employed. To assure precise prediction of deformation behavior including loading and unloading, the magnitude of the time increment is determined such that $\Delta u/L = (\dot{u}/L)\Delta t < 2.5 \times 10^{-4}$ for all computational processes.

4.2. *Results and discussion*

With $c_1 = c_2 = c_o$, the effect of the initial number of entanglements on the neck propagation behavior has been investigated for $m_o = m_a$, $m_a/2$ and $m_a/3$. Figure 10(a) shows the nominal stress versus elongation due to the present model and BPA model. The overall deformations are essentially the same as in the case predicted by the phenomenological constitutive equation (Neale and Tugcu, 1985; Tomita and Hayashi, 1993). The force attains the maximum value and then falls to the local minimum, with neck localization. Upon further straining, the neck stabilizes, and neck propagation takes place under approximately steady-state conditions. With a fixed number of total kinks N_A, the reduction of m_o yields an increase in the average number of kinks in a single chain, which causes the relative reduction of resistance to alignment. Furthermore, the reduction of m_o contributes to increase of the number of entanglements through eqn (13). Namely, corresponding values of $(1-m_o/m_u)$ and $(1-m_o/m_l)$ for $m_o = m_a$, $m_a/2$ and $m_a/3$ are 0, 1/2, 2/3 and -2, $-1/2$, 0, respectively. All of these lower the nondimensional stress, as shown in Fig. 10(a).

Figure 10(b) indicates the evolution of the radius of specimen R/R_o at cross-section 1 and the triaxiality factor F_T which is defined as the ratio of average representative stress to average axial stress through specimen cross-section 1. The relative radius of specimen R/R_o decreases uniformly as deformation proceeds and then drops sharply with neck formation. With neck propagation, it tends to a constant value. The triaxiality factor suddenly decreases as the load begins to drop from the maximum and attains the minimum. With further deformation, it increases and asymptotically tends to a constant value. Furthermore, as discussed by Tomita and Hayashi (1993), the triaxiality factor at cross-section 2 first

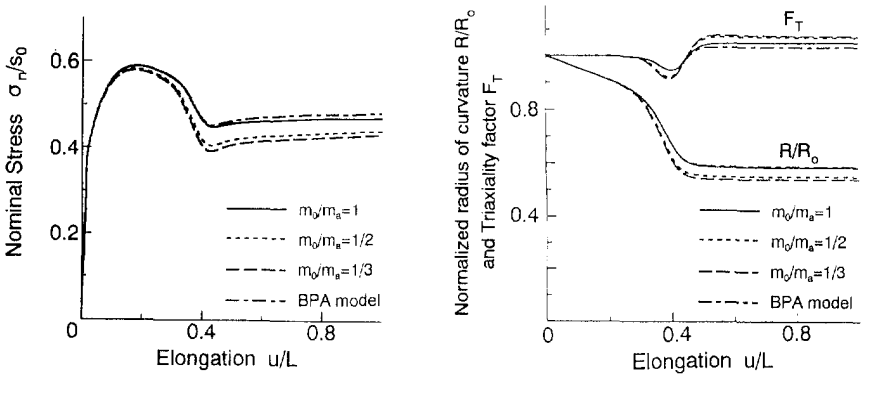

Fig 10. Effect of initial number of entanglements m_o on nominal stress versus elongation (a) and normalized radius and triaxiality factor versus elongation (b). BPA indicates the results based on the BPA model (Boyce *et al* 1988). Employed material parameters are the same as in Fig. 9 except m_o.

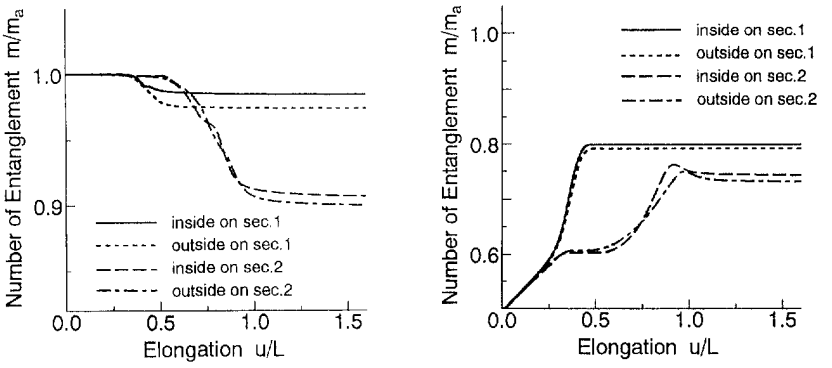

Fig 11. Nondimensional number of entanglements m/m_o versus elongation u/L for (a) $m_o/m_a = 1$ and (b) $m_o/m_a = 1/2$. The notation and material parameters employed are the same as for Fig. 9 except m_o.

increases to the maximum value and then decreases to the minimum as the neck propagates. Subsequently, it tends toward a constant value which is smaller than that of cross-section 1. The triaxiality factor at cross-section far from cross-section 1 behaves in much the same way as that at cross-section 2. This implies that the nonuniformity of deformation decreases as the cross-section approaches cross-section 1. Figure 10(b) suggests that a larger-sized neck propagates and triaxiality increases as m_o/m_a decreases.

Next, the evolution of the number of entanglements at different cross-sections and different positions has been investigated for $m_o/m_a = 1$ and $1/2$. Figure 11(a) shows the nondimensional number of entanglements at sections 1 and 2 in Fig. 9 for $m_o/m_a = 1$. Due to the shear deformation, the number of entanglements starts to decrease upon the onset of necking at cross-sections 1 and 2. The number of entanglements becomes constant when the deformation proceeds and necking stops. The reduction of the number of entanglements at section 2 is larger than that at section 1, which is consistent with the behavior of the triaxiality factor of cross-section 2. Figure 11(b) shows the number of entanglements versus elongation for $m_o/m_a = 1/2$. Considerable difference is observed compared with the case for $m_o/m_a = 1$. In this case, due to the contribution of normal strain on the increase of the number of entanglements [see eqn (13)], entanglements increase as the uniform deformation proceeds. The increase rate substantially changes with the onset of necking, which is attributed to the localization of deformation and the contribution of the second term of eqn (13). In cross-section 1, it rapidly increases up to the completion of necking. Subsequently, when the neck propagates to cross-section 2, the number of entanglements gradually increases to a maximum then slightly decreases and asymptotically tends to a constant value. In real polymeric material, the local number of entanglements is distributed so that depending on the local number of entanglements, it may increase or decrease as the deformation proceeds.

Finally, the effect of c_1/c_2 on the deformation behavior has been investigated. Figure 12(a) depicts the nominal stress versus elongation with $m_o/m_a = 1/2$, $c_1/c_2 = 1.0$ ($c_1 = c_2 = c_o$), $c_1/c_2 = 2.0$ ($c_1 = 2c_o$, $c_2 = c_o$) and $c_1/c_2 = 0.5$ ($c_1 = c_o$, $c_2 = 2c_o$). Comparison of these three cases clarified that the effect of c_2 on the deformation behavior is very small compared with that of c_1. This is attributed to the characteristic feature of the deformation in which the predominant deformation mechanism is tension and the contribution of the second term of eqn (14) is not very marked. Figure 12(b) shows the effect of c_1/c_2 on the number of entanglements at the outermost element on the cross-section 1. In all cases, since m_o is smaller than m_a the number of entanglements increases with the normal plastic strain, of which the tendency is magnified with increase of c_1/c_2. This can be explained by the above mentioned relation between the chain direction and induced strain. For $c_1/c_2 = 0.5$, the number of entanglements increases up to a maximum and the decreases to a steady state.

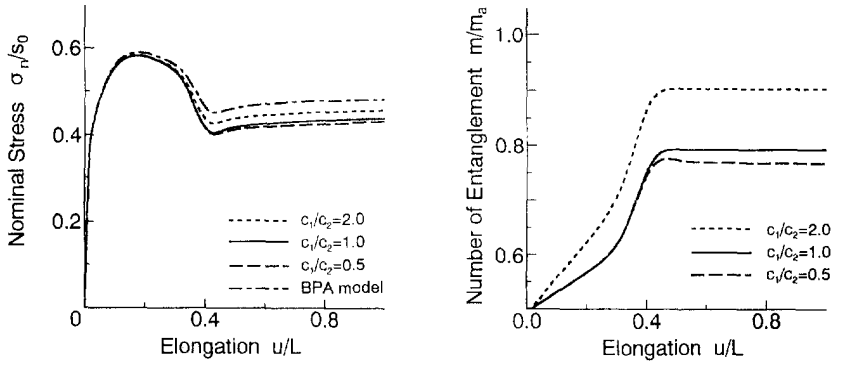

Fig 12. Effect of c_1/c_2 on nominal stress versus elongation (a) and number of entanglements versus elongation (b) for $m_0/m_a = 1/2$. The notation and material parameters employed are the same as for Fig. 9 except m_0 and c_1/c_2 values.

5. CONCLUSIONS

With the non-Gaussian network model and generalized Argon double-kink model of intermolecular resistance, a three dimensional constitutive equation for polymeric materials has been developed. A simple relation between the non-Gaussian molecular chain network structure and the number of entanglements of chains is formulated and a simple evolutional equation for the number of entanglements of chains during the deformation process is developed. Through the comparison between the predicted results and experimentally obtained results, it has been proven that the proposed constitutive equation has the capability to duplicate the deformation behaviors under different stress conditions given a set of material parameters.

As an application of the proposed constitutive equation, the tension of cylindrical bars has been investigated, and the effect of the initial number of entanglements and the type of evolutional equation of the number of entanglements on the neck propagation behavior has been briefly discussed.

Acknowledgements—Support for the present work was provided by the Ministry of Education, Science and Culture of Japan.

REFERENCES

Argon, A. S. (1973). A theory for the low-temperature plastic deformation of glassy polymers. *Phil. Mag.* **28,** 839–865.

Arruda, E. M. and Boyce, M. C. (1991). Evolution of plastic anisotropy in amorphous polymers during finite straining. In *Anisotropy and Localization of Plastic Deformation* (Edited by J.-P. Boehler and A. S. Khan), pp. 483–488. Elsevier Applied Science, London.

Arruda, E. M. and Boyce, M. C. (1993a). A three dimensional constitutive model for large stretch behavior of rubber materials. *J. Mech. Phys. Solids* **41,** 389–412.

Arruda, E. M. and Boyce, M. C. (1993b). Evolution of plastic anisotropy in amorphous polymers during finite straining. *Int. J. Plast.* **9,** 697–720.

Botto, P. A., Duckett, R. A. and Ward, I. M. (1987). The yield and thermoelastic properties of oriented poly(methyl methacrylate). *Polymer* **28,** 257–262.

Boyce M. C. and Arruda, E. M. (1990). An experimental and analytical investigation of the large strain compressive and tensile response of glassy polymers. *Polym. Engng Sci.* **30,** 1288–1298.

Boyce, M. C., Parks, D. M. and Argon, A. S. (1988). Large inelastic deformation of glassy polymers. I. Rate dependent constitutive model. *Mech. Mater.* **7,** 15–33.

Chater, E. and Hutchinson, J. W. (1984). Mechanical analogs of coexistent phases. In *Phase Transformation and Material Instabilities in Solids* (Edited by M.E. Gurtin), pp. 21–36. Academic Press, New York.

Fager, L. O. and Bassani, J. L. (1986). Plane strain neck propagation. *Int. J. Solids Struct.* **22,** 1243–1257.

G'Sell, C. and Gopez, A. J. (1985). Plastic banding in glassy polycarbonate under plane strain shear, *J. Mat. Sci.* **20,** 3462–3478.

Hutchinson, J. W. and Neale, K. W. (1983). Neck propagation. *J. Mech. Phys. Solids* **31,** 405–426.

Neale, K. W. and Tugca, P. (1985). Analysis of necking and neck propagation in polymeric materials. *J. Mech. Phys. Solids* **33,** 323–337.

Tanaka, S. and Tomita, Y. (1993). A constitutive modelling of glassy polymers based on molecular chain network model considered internal structural transformation and its application. *Proc. 17th NCP Symp.* pp. 9–10.

Tomita, Y. (1994). Constitutive modeling of mechanical characteristics of materials and computational simulation of plastic instability behaviors, *Proc. 37th JCMR*. pp. 1–9. The Society of Materials Research, Japan.

Tomita, Y., Takahashi, T. and Shindo, A. (1990). Neck and bulge propagation in polymeric cylinders. *Int. J. Mech. Sci.* **32,** 335–343.

Tomita, Y. and Hayashi, K. (1991). Deformation behavior in elasto-visoplastic polymeric bars under tension, *Proc. Plasticity* **91,** 524–527.

Tomita, Y. and Hayashi, K. (1993). Thermo-elasto-viscoplastic deformation of polymeric bars under tension. *Int. J. Solids Struct.* **30,** 225–235.

Tomita, Y. and Tanaka, S. (1994). Prediction of deformation behavior of glassy polymers based on molecular chain network model, *WCCM III*, pp. 588–589.

Tugcu, P. and Neale K. W. (1987a). Necking and neck propagation in polymeric materials under plane strain tension. *Int. J. Solids Struct.* **23,** 1063–1085.

Tugcu, P. and Neale, K. W. (1987b). Analysis of plane-strain neck propagation in viscoplastic polymeric films. *Int. J. Mech. Sci.* **29,** 793–805.

Tugcu, P. and Neale, K. W. (1988). Analysis of neck propagation in polymeric fibers including the effect of viscoplasticity. *Trans. ASME. J. Eng. Materials Tech.* **110,** 395–400.

Tugcu, P. and Neale, K. W. (1990). Cold drawing of polymers with rate and temperature dependent properties. *Int. J. Mech. Sci.* **32,** 405–416.

Wu, P. D. and van der Giessen, E. (1993a). On improved network models for rubber elasticity and their applications to orientation hardening in glassy polymers. *J. Mech. Phys. Solids* **41,** 427–456.

Wu, P. D. and van der Giessen, E. (1993b). Analysis of shear band propagation in amorphous glassy polymers. *Int. J. Solids Struct.* **31,** 427–456.